RSC Advances

ROYAL SOCIETY OF CHEMISTRY

PAPER

View Article Online
View Journal | View Issue



Cite this: *RSC Adv.*, 2023, **13**, 5134

# Spirocyclic rhodamine B benzoisothiazole derivative: a multi-stimuli fluorescent switch manifesting ethanol-responsiveness, photo responsiveness, and acidochromism†

Himabindu Battula,[a] Moromi Nath,[b] Sabyashachi Mishra[b] and Subbalakshmi Jayanty *[a]

Multi-stimuli fluorescent switching materials have been extensively employed in chemistry, biochemistry, physics, and materials science. Although rhodamine-based spirolactams have been specifically considered for metal ion sensing by photoluminescence, only some of them manifest photochromic behavior, and further development of rhodamine B (RHB)-based photochromic materials is required. RHB and its cyclic amides are advantageous in various sensing applications owing to their colorimetric responses to external stimulation. Hence, the current work reports a novel multifunctional active molecular material (3′,6′-bis(diethylamino))-2-(5-nitrobenzo[c]isothiazol-3-yl)spiro[isoindoline-1,9′-xanthen]-3-one (**RHBIT**) by linking rhodamine B with 3-amino,5-nitro[2,1]benzoisothiazole (ANB) in a facile synthetic pathway; that perceives both emission color change and switching between off–on states. **RHBIT** shows acidochromism, photochromism, and pH sensitivity accompanied by unique ethanol responsiveness, with potential applications in anti-counterfeiting and drug delivery. Notably, **RHBIT** is highly acid sensitive and reverts to the ring-closed form on treatment with triethylamine (base), visible with the naked eye amidst colorless–pink–colorless transformations. On short UV irradiation, **RHBIT** provides a two-fold rise in the lifetime for the ring-open form in $CHCl_3$ and DCM compared to the spirolactam (closed form). DFT and TDDFT studies provide electronic characterization for the absorption spectra of the open and closed forms. Using the photoresponsive feature of **RHBIT**, an information protection application has been enacted *via* a rewritable platform.

Received 16th December 2022
Accepted 24th January 2023

DOI: 10.1039/d2ra08022b

rsc.li/rsc-advances



## 1 Introduction

Photoresponsive materials have attained great importance due to their potential applications as fluorescence sensors,[1] photo-controllable switches,[2] memory devices,[3] and in super-resolution spectroscopy[4] and volumetric displays.[5] Multi-stimuli-responsive materials have been established in diverse fields like photoresponsive chemosensors,[6] photodynamic therapy,[7] photopatterning,[2] and photoacoustic imaging.[8] Hitherto, multifunctional photoresponsive materials were developed by introducing various stimuli, including pH, light, heat, solvent, mechanical force, and electric fields.[9,10] Among these, light is a peerless stimulus due to its explicit properties like unambiguous stimulation besides its response, eco-friendliness, and remote non-destructive control. To date, photoresponsive molecular systems like spiropyrans, diarylethenes, azobenzenes, spirooxazine, viologen, *etc.*, have experienced color changes by photoirradiation and been used in various fields such as physical, chemical, biological, optical, and nanotechnology.[11–13] Nevertheless, rhodamine B (RHB), a class of xanthene dye with excellent spectroscopic properties, quantum efficiency, and good photostability, and a well-known sensitive switching material, undergoes fluorescence changes due to its reversible isomerization between open-ring (fluorescent) and closed-ring (non-fluorescent) forms in solution, with other surrounding conditions and sustainability, and has been used to sense metal ions in environmental samples.[14] Recently, we detected that certain open-chain amide derivatives of RHB exhibited a dual effect of fluorescence and anticancer activity.[15]

Cyclized spirolactam is non-fluorescent due to interruption of conjugation in the xanthene moiety, while the reversible structural transition from a non-fluorescent representative form to a highly fluorescent zwitterionic form is influenced by pH, solvent polarity, and ultraviolet irradiation. Such reversible off–

[a]*Department of Chemistry, Birla Institute of Technology and Science, Pilani-Hyderabad Campus, Jawaharnagar, Shameerpet, Kapra Mandal, Medchal Dist., Hyderabad-500078, Telangana State, India. E-mail: jslakshmi@hyderabad.bits-pilani.ac.in; Fax: +91-040-66303998; Tel: +91-40-66303561*

[b]*Department of Chemistry, Indian Institute of Technology, Kharagpur-721302, India*

† Electronic supplementary information (ESI) available. CCDC 2202193. For ESI and crystallographic data in CIF or other electronic format see DOI: https://doi.org/10.1039/d2ra08022b

on behavior facilitates the importance of rhodamine spirolactams in sensing/dye activation off–on switching applications. Therefore, rhodamine B derivatives are promising candidates for contriving multifunctional fluorescent switches, and so far much effort has been put into constructing them.[16,17]

Gleiter *et al.* first disclosed the photochromic features of *N*-aryl spirolactam rhodamines which transform between off–on states by UV illumination, with color changes persisting for milliseconds to minutes depending upon the solvent medium.[18] Hell *et al.* introduced a photoactivatable rhodamine phthalimide spirolactam into localization-based super-resolution imaging.[19] Li *et al.* provided a new strategy for developing multifunctional photoresponsive materials of a 2,4-dihydroxybenzaldehyde rhodamine B hydrazone Schiff base with metal complexes as reversible, photoresponsive systems which were favorable for constructing photocontrolled logic gates with tunable performance.[17] Recently, Zhiyong *et al.* brought about remarkable multi-stimuli-responsive behaviors, including a protonation effect, photochromism, and piezochromism with significant color changes of iso-*cis*/*trans*-aminobenzopyranoxanthenes as potential candidates for sensors, indicators, and detectors.[9] Murugesapandian *et al.* reported an excited-state intramolecular proton transfer (ESIPT)-active multi-functional molecular switch, a coumarin rhodamine B hydrazine-based material that exhibits methanol responsiveness and reversible photochromic feature of its zinc ensemble in the presence of a 365 nm UV lamp.[16] Very recently Fogerty *et al.* designed and synthesized a dual spirolactam moiety utilizing *p*-phenylene diamine that exhibited sensitivity to both pH and UV illumination; solvatochromic fluorescence emission was centered in the blue region of the spectrum, but an explanation of the linker chemistry that influences the open–closed equilibrium as well as solvatochromic emission in the dimer is lacking.[20] This color change is instantaneous in the case of chloroform and takes place over a few hours in the case of dichloromethane.

The transition of rhodamine spirolactams between the closed and open ring forms by pH sensitivity and UV light irradiation (~250–400 nm) depends on the steric and electron-withdrawing/releasing nature of the substituent groups attached to the nitrogen of the amide.[4,5,21] Generally, p$K_a$ values increase when there is an increase in the size and electron-withdrawing character of the substituent group; furthermore, smaller electron-withdrawing groups favor faster ring-opening kinetics and show an open form of the spirolactam in equilibrium.[22] Ring-opening kinetics also depend on solvent polarity and acidity; acidic solvents mostly favor the open form of rhodamine spirolactams.[5,21] In this context, Ma *et al.* reported a multi-stimuli-responsive rhodamine tetraphenylethylene (RHTPE) exhibiting aggregation-induced emission (AIE), methanol responsiveness, selectivity, photochromism, and mechanochromism.[23] The photoresponsive properties of RHTPE were studied in ethanol, chloroform and DMSO solvents (red emissive) under 365 nm UV light, and the solutions returned to colorless when the UV light was removed. Interestingly, though spirolactams have been explored especially for metal ion sensing through photoluminescence, only a few exhibited photochromic behavior and acid-sensing (HCl, $HNO_3$, picric acid, TFA, *etc.*) as mentioned above. It should be noted, that *p*-toluenesulfonic acid (**PTSA**) is an efficient catalyst in organic synthesis and is widely used as a counterion for basic drugs in the pharmaceutical industry owing to its strong acidic and hydrophilic properties; therefore, determining the content of **PTSA** in drug substances is a prerequisite for drug quality control and authenticity testing. Several analytical methods utilized for the detection of **PTSA** in drug and environmental samples are sophisticated and need expensive instruments.[24] Hence, an alternative fluorescence sensing method has become more prominent due to its high sensitivity and selectivity, operational lucidity, low cost, less time, and visible naked-eye detection.

Accordingly, we have chosen 3-amino,5-nitro[2,1] benzoisothiazole (ANB) possessing rich π-conjugation and an electron-withdrawing group; to investigate its emerging optical characteristics. In one of our earlier reports, ANB with **PTSA** resulted in a protonated charge transfer complex.[25] Nonetheless, interestingly, in the current study, we synthesized non-fluorescent (3′,6′-bis(diethylamino))-2-(5-nitrobenzo[*c*]isothiazol-3-yl)spiro[isoindoline-1,9′-xanthen]-3-one (**RHBIT**) spirolactam that exhibits spectacular properties, such as acidochromism, solvatochromism, and photochromic properties, especially by itself. The presence of an electron-withdrawing group (–$NO_2$) in ANB possibly favored a faster ring-opening mechanism and generated a highly fluorescent open form of **RHBIT** under acid and UV irradiation stimuli. Henceforth, in this article, we present a comprehensive study on the photophysical and photoresponsive attributes of an easily acquired novel rhodamine cyclized spirolactam **RHBIT** (obtained by linking ANB to RHB through a facile synthesis); with a crystal description, and its sensing application with **PTSA** in solution. This study will perhaps contribute to the development of multi-stimuli-responsive materials which can be successfully applied for multicolor inks, sensors, photo printing, displays, and biological imaging.

## 2 Experimental section

### 2.1 Materials

All reagents were procured from commercial suppliers indicated below (in brackets) and used without further purification: rhodamine B (Sigma-Aldrich), 3-amino,5-nitro[2,1] benzoisothiazole (Sigma Aldrich), 1-hydroxybenzotriazole (HOBT) (Spectrochem Pvt. Ltd.), 1-(3-dimethylaminopropyl)-3-ethyl carbodiimide hydrochloride (EDC.HCl) (Spectrochem Pvt. Ltd.), *N*,*N*-diisopropylethylamine (DIPEA) (Spectrochem Pvt. Ltd.), *N*,*N*-dimethylformamide (DMF) (SRL Pvt. Ltd.), dichloromethane (DCM) (SRL Pvt. Ltd.), acetonitrile (SRL Pvt. Ltd.), absolute ethyl alcohol (Hychem Laboratory), *p*-toluene sulfonic acid monohydrate (**PTSA**) (SRL Pvt. Ltd.) recrystallized in acetonitrile for further use. Column chromatography was accomplished using 60–325 mesh neutral alumina. Reactions were monitored by thin layered chromatography (TLC) on $F_{254}$ plates (Merck & Co.) pre-coated with silica gel 60 G; visualized by a UV lamp.

### 2.2 Methods and measurements

FT-IR spectra were taken on a Shimadzu IR Affinity-1S FTIR (400–4000 $cm^{-1}$) using KBr as a matrix. Electron spray ionization mass spectroscopy (ESI-MS) was acquired on a Shimadzu LCMS-8040. $^1H$, and $^{13}C$ NMR spectra were recorded on a Bruker Advance DRX (400–500 MHz) with deuterated chloroform solvent; and tetramethylsilane (TMS) as the internal standard. $CDCl_3$ (7.26 ppm in $^1H$ and 77.2 ppm in $^{13}C$) and chemical shifts are reported in ppm, and multiplicities are shown as s (singlet), d (doublet), t (triplet), q (quartet), dd (doublet of doublet), or br (broad). The absorption measurements of **RHBIT**, before and after UV irradiation, were done on a JASCO V-650 spectrophotometer. Emission studies and quantum yield measurements were carried out on Fluorolog–Horiba, using a 1 cm path length quartz cuvette with an excitation/emission slit width of 2 nm. Solid UV absorption studies were measured on a JASCO V-670 (UV-VIS NIR) spectrophotometer. Time-resolved fluorescence measurements were recorded using a time-correlated single-photon counting (TCSPC) Horiba DeltaFlex Modular fluorescence system using the instrumental parameters: 375 nm, 510 nm nano LED excitation source, bandpass of 4 nm, peak preset of 10 000 counts; the time resolution was 25 ps. All measurements were performed at room temperature. The effect of pH was studied using a digital pH meter (LI 120 – Elico M) equipped with a glass electrode.

The morphology of drop-casted films for **RHBIT** on a silicon wafer with gold sputtering was studied under an Oxford X-max$^N$ LEICA EM ACE200 scanning electron microscope. The silicon wafers were washed thoroughly with water and acetone and dried in an oven at 100 °C before use. Thermogravimetric analysis (TGA)-differential thermal analysis (DTA) was carried out on a Shimadzu DTG-60 simultaneous DTA-TG instrument with an increase in temperature at a rate of 10 °C $min^{-1}$ from 30 °C to 700 °C under an $N_2$ atmosphere. Differential scanning calorimetry (DSC) was recorded on a Shimadzu DSC-60 instrument under similar conditions to those mentioned above with a temperature range of 30 °C to 350 °C.

### 2.3 Synthesis and characterization

**2.3.1 (3′,6′-Bis(diethylamino))-2-(5-nitrobenzo[*c*]isothiazol-3-yl)spiro[isoindoline-1,9′-xanthen]-3-one; RHBIT.** In a 25 mL round-bottomed flask, RHB (0.1 g, 0.2 mmol) was dissolved in 3 mL of DMF at 0 °C under an $N_2$ atmosphere followed by the addition of DIPEA (0.051 g, 0.4 mmol). The reaction was stirred for 10 min, then HOBT (0.054 g, 0.4 mmol) and EDC·HCl (0.076 g, 0.4 mmol) were added and stirred at 0 °C for about 20 min. Later ANB (0.12 g, 0.6 mmol) was added to the resulting mixture and stirred at 20 °C, for another 16 h (ref. 14) (Scheme 1). After completion of the reaction (monitored by TLC), 15 mL of cool water was added to the resultant mixture and left for some time. After 20 min a solid formed at the bottom of the flask, which was filtered through a vacuum and dried in a desiccator. A purple solid was obtained. It was purified by column chromatography on neutral alumina using DCM solvent alone. The final product **RHBIT** was collected immediately after 2 fractions as a single spot in TLC and was evaporated, resulting in a yellow solid with (0.078 g) 65% yield. Subsequently, the yellow solid was dissolved in a 3 : 2 ratio acetonitrile : ethanol mixture, heated at 50 °C for 5–10 minutes, and evaporated slowly at room temperature. Within ~48 h, clear brownish blocks of **RHBIT** single crystals could be obtained. mp 290–293 °C, ESI-MS $m/z^+$ calculated for $C_{35}H_{33}N_5O_4S$: 619.23, found ($[M + H]^+$) 620 (Fig. S1†); HRMS (EI): $C_{35}H_{33}N_5O_4S$ $[M + H]^+$ calcd $m/z$: 619.23; found $m/z$: 620 (Fig. S2†). IR ($\nu_{max}/cm^{-1}$) as KBr pellets: 2968 (–C–H s), 1716 (–C=O s), 1610 (–C=C s), 1515 (–C–$NO_2$), 1411 (–C–H b), 1335, 1214, 1122 (C–N s), 882, and 815 (–C–S s) $cm^{-1}$ (Fig. S3†). $^1H$ NMR (400 MHz, $CDCl_3$) $\delta$ 8.55 (d, 1H, $J = 1.9$ Hz, Ar–H), 8.03–8.00 (dd, 1H, Ar–H), 7.97 (dd, 1H, $J = 9.7$, 2.3 Hz, Ar–H), 7.55–7.47 (m, 3H, Ar–H), 7.15 (dd, 1H, $J = 6.4$, 1.3 Hz, Ar–H), 6.60 (d, 2H, $J = 8.9$ Hz, Ar–H), 6.28 (d, 2H, $J = 2.5$ Hz, Ar–H), 6.22 (dd, 2H, $J = 8.9$, 2.6 Hz, Ar–H), 3.24 (q, 8H, $J = 7.2$ Hz, –$CH_2$), 1.06 (t, 12H, $J = 7.1$ Hz, –$CH_3$) (Fig. S4†). $^{13}C$ NMR (101 MHz, $CDCl_3$) $\delta$ 164.6, 162.1, 158.9, 152.6, 152.4, 148.5, 142.3, 133.4, 127.8, 127.2, 123.3, 123.1, 121.5, 120.8, 120.3, 107.5, 102.6, 97.0, 68.4, 43.3, 11.4 (Fig. S5†). The molecular structure of the cyclic **RHBIT** was confirmed by single crystal X-ray study with corresponding CCDC No. 2202193.†

### 2.4 Crystallographic data and refinement

Selected suitable single crystals of **RHBIT** were mounted on a Rigaku XtaLAB P200 diffractometer at 100 K with graphite monochromated Cu-Kα radiation ($\lambda = 1.54184$ Å). CrysAlisPro (Rigaku Oxford Diffraction) software was used to collect and reduce the data. The Olex2 (ref. 26) with ShelXT[27] structure solution program was used to solve the structure, and the ShelXL[28] refinement package was used to refine the data. Basic crystallographic data is tabulated in Table S1 (ESI).† Complete crystallographic details are given in the ESI (Tables S2–S7†).

### 2.5 UV-vis absorption and fluorescence measurements

The stock solution was prepared by weighing 1 mg of **RHBIT** (100 ppm) dissolved in 10 mL of acetonitrile solvent and further diluted to 25 ppm (40 μM) for absorption and emission studies. For the Job plot experiment, a total concentration of 100 μM of **RHBIT** and **PTSA** solutions (where the mole fraction of **PTSA** varied from 0 to 1) was considered. For the pH study, 500 μL of (25 ppm) **RHBIT** was taken and mixed with 1500 μL of different pH solutions (pH = 2 to 10), prepared by using standard buffer capsules with pH 4,7 and 9; further adjusted to acidic and basic conditions using small volumes of 2 M HCl or 2 M NaOH solutions. The corresponding absorption and emission spectra were recorded at various pH conditions. Solvatochromic and other sample pictures were captured by a cellphone camera.

### 2.6 Computational details

The cyclic and open structures of **RHBIT** were modeled in Gaussview[29] and optimized using density functional theory[30] in the Gaussian16 software package.[31] The optimization and frequency calculations were done using the ωb97XD functional[32] and 6-31G(d,p) basis set[33] for all atoms. Molecules were

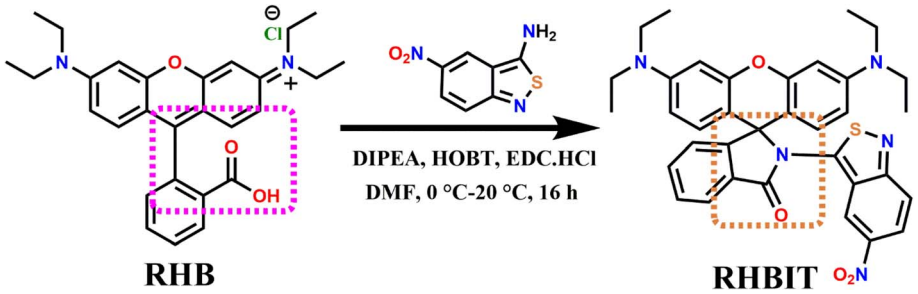


Scheme 1 Facile and single-step synthetic route for the preparation of compound RHBIT.

optimized without any geometric or symmetry constraint in the gas phase. Analytic frequencies were computed to confirm the minima of all stationary points. The HOMO–LUMO energy difference was calculated from the minimum-energy structure. TDDFT calculations were employed to obtain the vertical excitation energy and oscillator strength (representing the absorption intensity) at the ground-state optimized geometry. The natural transition orbitals were determined using the Multiwfn program.[34]

## 3 Results and discussion

**RHBIT** could be achieved by a facile synthesis in a single step (Scheme 1), by modification of our previously reported procedure.[14] The chemical structure was confirmed from spectroscopic data (Fig. S1–S5†), and **RHBIT** was found to be thermally stable under ambient conditions with a decomposition temperature of ~294 °C. The explored results are fortified by fluorescence lifetime and quantum yield measurements. The basic conception of acid-sensing is explained by fluorescence-based titration studies. The molecular functionality of **RHBIT** was confirmed by a new characteristic peak at 1716 $cm^{-1}$, which corresponds to the carbonyl stretching frequency of lactam, and 2968 $cm^{-1}$ attributed to the C–H stretching of a methylene group.[35] A shift in the wavenumber from 1591 $cm^{-1}$ in RHB (–C═O) to 1716 $cm^{-1}$ (–C═O) in **RHBIT** (Fig. S3†) indicates the formation of spirolactam. The cyclized structure was also supported by a characteristic signal in the $^{13}C$ NMR spectrum near 68.48 ppm (spiro-carbon) (Fig. S5†), representing the formation of 3° carbon of **RHBIT** in deuterated chloroform.[36] The spirolactam (–C═O) group appeared at $\delta = 162.09$ ppm in the $^{13}C$ NMR spectrum. The above interpretations clearly confirmed that **RHBIT** existed in the closed-ring spirolactam form (Scheme 1).

### 3.1 Crystallography study

A molecular ORTEP diagram with a 50% probability of thermal ellipsoids is shown in Fig. 1(a). A crystallography study of **RHBIT** reveals the unique spirolactam ring structure at N8–C58–C57; N3–C7–C22 in (Fig. 1(a)); also supported by the characteristic peak of 68.48 ppm (spiro-carbon) in the $^{13}C$ NMR spectrum (Fig. S5†). **RHBIT** crystallized in the monoclinic *P*21 space group. The asymmetric unit (Fig. S6(a)†) contains two complete **RHBIT** units each with an empirical formula $C_{35}H_{33}N_5O_4S$. The angle between the planes of the xanthene ring and the spirolactam moiety is found to be 87.58° (Fig. S6(b)†), slightly twisted when compared to RHB, wherein

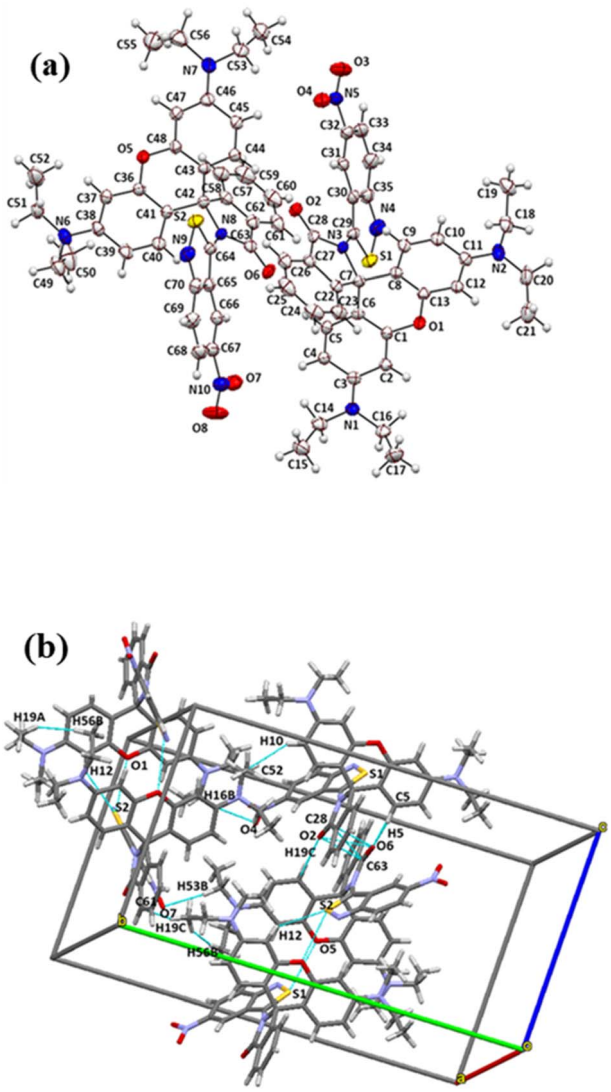


Fig. 1 (a) ORTEP diagram of **RHBIT** showing 50% probability thermal ellipsoids. (b) Prominent short contacts within the range 2.249 Å to 3.373 Å manifested between the **RHBIT** molecules.

the angle between the xanthene and the phenyl ring with carboxylic acid functionality is 90° in RHB; while the angle between the planes of the spirolactam unit and the ANB moiety is observed to be 42.54° (Fig. S6(c)†); the angle between ANB and the xanthene ring planes is 81.15° (Fig. S6(d)†). The torsion angle between C6, C7, C22, and C23 is 63.33°; that between C8, C7, N3, and C29 is 67.57°. Despite extensive short contacts (<sum of van der Waals radii) in the range of 2.249 Å to 3.373 Å existing in **RHBIT** units, prominent short contacts (Fig. 1(b)) were between O2···O6 (2.992 Å), C28···C63 (3.373 Å), S1···O5 (3.190 Å), O1···S2 (3.179 Å), H12···S2 (2.989 Å), H53B···O7 (2.679 Å), C5···O6 (3.075 Å), C52···H10 (2.764 Å), O2···H44 (2.249 Å), H19A···H56B (2.357 Å), and C61···H19C (2.851 Å). The anti-parallel alignment of the **RHBIT** moiety was noticed along the axes *ob* and *oc*, while parallel arrays were observed along the *oa* axis (Fig. S6(e)†).

### 3.2 Effect of pH

Rhodamine spirolactam derivatives are well-known fluorescent pH sensors under acidic conditions *via* the ring-opening process by protonation. However, **RHBIT** exhibits very weak absorption and emission in the pH range of 6–10 in the acetonitrile–water system and exists as a spirocyclic form that is colorless and non-fluorescent. As the pH value decreased (<5), an increase in the intensity of the absorption band at $\lambda_{max} \sim 564$ nm was observed and the colorless solution of **RHBIT** quickly turned pink due to the ring-opening mechanism induced by the proton. Additionally, emission spectra resemble the same response at pH < 5 and show high emission intensity at ∼575 nm wavelength. While increasing the pH > 6 by subsequent addition of NaOH resulted in a colorless solution, very weak emission in alkaline solution at ∼575 nm was observed. This implies reversible coordination between **RHBIT** and $H^+$ where the spectral and color changes showed that **RHBIT** can probe pH reversibly, and this detection process is visible to the naked eye. However, the emission wavelength of the probe gradually increased with a ∼19 nm bathochromic shift from 575 nm to 594 nm at pH 2. Also, the fluorescence emission intensity at lower pH (2) was ∼18-fold larger than that at higher pH (10). Moreover, pH-dependent variations were measured to estimate the stability of the spirolactam moiety. Remarkable changes in emission intensity were only perceived below pH 6, and the spirocyclic form of **RHBIT** was stable in the pH range 6–10 (Fig. S7†). The observed stability of the spirolactam ring should enable **RHBIT** to be suitable for bioassays since most biofluids have a pH of ∼7.4. Hence, **RHBIT** can be considered an effective fluorescence "turn-on" sensor for pH detection under more acidic conditions. Interestingly, a similar phenomenon was remarked in a rhodamine 6G hydrazide derivative[37] and it was proposed for the detection of pH levels in the human stomach/certain acidic environments.

### 3.3 Optical studies

**3.3.1 Ethanol responsiveness of RHBIT.** Initially, the solvatochromic behavior was studied by dissolving **RHBIT** (25 ppm) in 12 common organic solvents, which demonstrated unique sensitivity with respect to solvent polarities. **RHBIT** was more soluble in chlorinated solvents, such as chloroform and dichloromethane, compared to polar protic or aprotic solvents. Interestingly, **RHBIT** solutions were colorless in the rest of the solvents, except that ethanol showed a pink color in ambient light (Fig. 2(a1)), indicative of **RHBIT** as an ethanol-responsive molecule. To ascertain the reason behind the distinct color change in ethanol; absorption and emission measurements were investigated in 12 different solvents, and the results obtained are shown in Fig. 2. The UV-vis absorption spectra showed absorption peaks of ∼389 nm for the cyclized form of **RHBIT** in almost all solvents considered, except for ethanol (Fig. 2(a)). In ethanol, along with a 409 nm peak, an apparent sharp intense absorption peak at 560 nm was noted, compared to *n*-propanol and *n*-butanol (at 554 nm), which was accountable for the observed pink color in ethanol, suggesting that ethanol is favorable to ring-open species of **RHBIT**. There is no evident peak in the 560 nm range for aprotic solvents where only a 389 nm ($n \rightarrow \pi^*$ transition) peak is perceived. At the excitation wavelength of 340 nm, **RHBIT** exhibits dual emission in all the solvents quoted above (∼400 nm, ∼428 nm); except for ethanol (∼429 nm and ∼589 nm) (Fig. 2(b)). Indeed, the fluorescence spectra display a strong emission band with high intensity at ∼589 nm only in ethanol, verifying the isomerization of closed and open forms in ethanol, owing to the strong hydrogen-bonding interactions of the aminobenzoisothiazole moiety. A similar phenomenon was observed by Bag *et al.*, where a rhodamine-based FRET signaling system with a nitrobenzoxadizole fluorophore amidst an acyclic amino receptor displayed prominent absorption and emission intensities in protic solvents like MeOH, EtOH, and $H_2O$ due to the possible H-bonding interactions with the receptor, revealing a key role in the ring-opening process.[38] Moreover, Wang *et al.* reported that (i) the strong polarity of the solvents is favorable for intramolecular charge separation in its ring-open state and further stabilized by strong electron-withdrawing groups; (ii) strong H-bonding interactions of the protic solvents with the amide moiety perhaps giving stability to the ring-open form of cyanorhodamine spirolactams.[39] Generally, a low p$K_a$ value hastens the isomerization rate of ring closed and open forms, and high polarity stabilizes the conjugated zwitterion with a large dipole moment.[23] The p$K_a$ of ethanol is 15.9, and the polarity value is 0.65, closer to the p$K_a$ (15.6) and polarity of methanol (0.76), and comparatively higher than other solvents according to CRC Handbook[40] (Table 1). The pH value of **RHBIT** in ethanol is ∼4.4 before exposure to 254 nm UV light, which is under acidic conditions when juxtaposed with other solvents. As mentioned in Section 3.2, highly acidic conditions favor the ring-opening mechanism of spirocyclic **RHBIT**. Thus, **RHBIT** manifests good ethanol responsiveness due to its lower pH value and strong H-bonding interactions with ethanol. This is hardly seen in rhodamine derivatives and it exists as a spironolactone (colorless solution) form in aprotic solvents.

**3.3.2 Photoinduced absorbance and fluorescence emission of RHBIT in different solvents.** Irradiation of **RHBIT** in varied solvents under short-wavelength UV (254 nm) light surprisingly led to an instantaneous color change, *i.e.* from colorless to

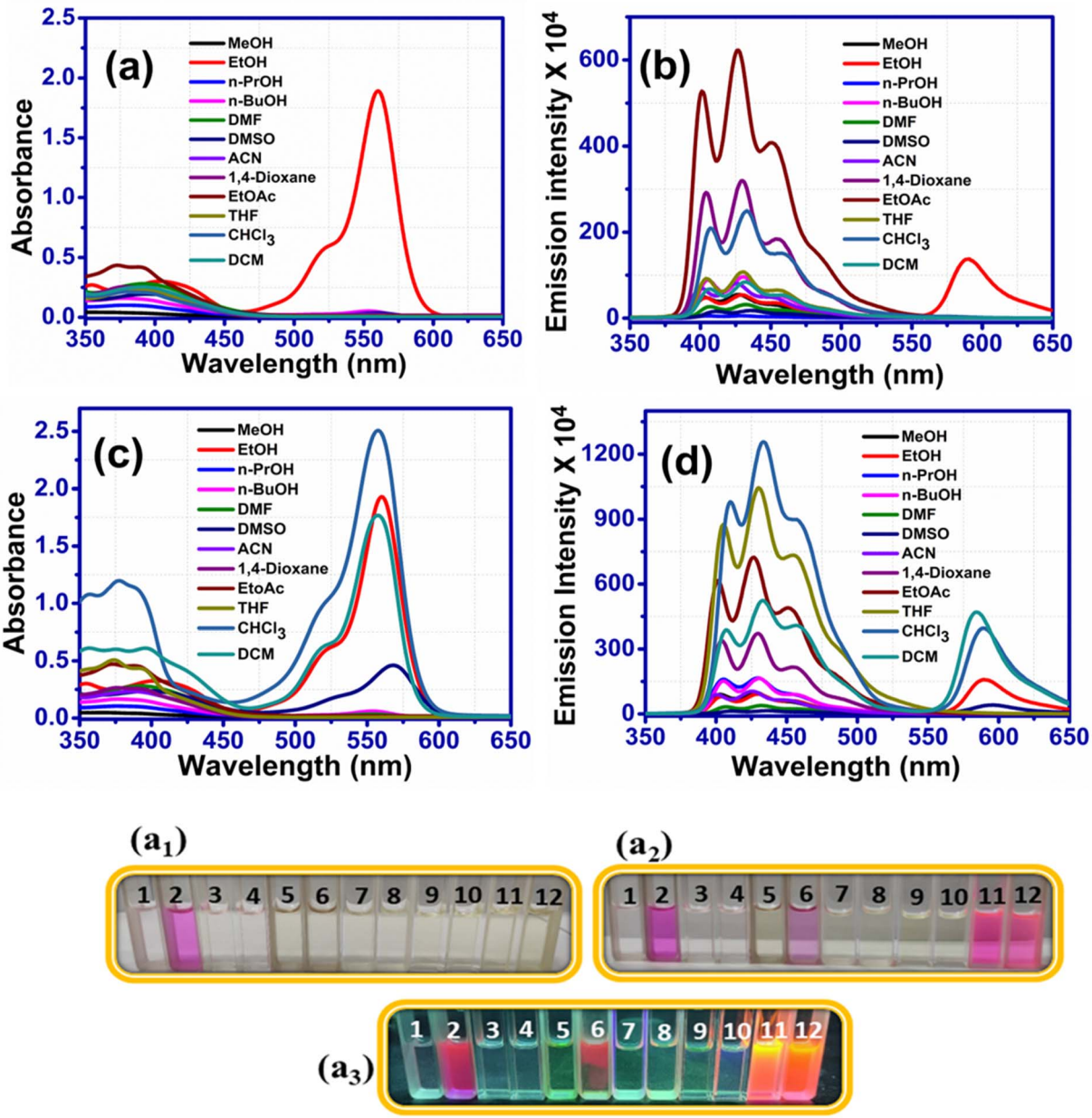


Fig. 2 Absorption and emission spectra of **RHBIT** in different solvents (40 μM, $\lambda_{ex}$ = 340 nm): (1) methanol, (2) ethanol, (3) *n*-propanol, (4) *n*-butanol, (5) DMF, (6) DMSO, (7) ACN, (8) 1,4-dioxane, (9) ethyl acetate, (10) THF, (11) $CHCl_3$, (12) DCM; representing (a) absorption and (b) emission spectra before UV irradiation; similarly (c) absorption and (d) emission spectra after UV irradiation. Photographic images taken under ($a_1$) ambient light for **RHBIT** before UV exposure and ($a_2$) after UV exposure; where ($a_1$) shows **RHBIT** appearing as pink in ethanol solvent and colorless in the remaining solvents under ambient light. ($a_3$) Presents a photographic image of ($a_2$) taken under short-wavelength UV light (254 nm). ($a_2$) and ($a_3$) depict the color transformation of **RHBIT** from colorless to pink/orange in DMSO, chloroform, and DCM solvents when observed under short-wavelength UV (254 nm) illumination.

orange fluorescence, in less than 1 min primarily in chloroform, after 5 min in DCM and ~20 min in DMSO and remained unchanged (pink color) in ethanol solvent (Fig. 2(a2) and (a3)). Such a color change was not observed in the presence of long-wavelength UV (365 nm) or with other solvents. The absorption and emission spectra were recorded before and after exposure to UV light. The vibronic absorption spectrum of the orange-colored species is very similar to that of the zwitterionic species of **RHBIT**.[18]

**RHBIT** showed absorbance at ~560 nm for protic solvents and no absorbance above ~450 nm (Fig. 2(a)) before UV light irradiation for aprotic solvents. Fig. 2(b) presents emission spectra before UV irradiation. Interestingly, after UV light (of 254 nm) irradiation for 15–20 min of **RHBIT** in various solutions, intense absorbance peaks were noticed only in chloroform (~557 nm), DCM (~558 nm), and DMSO (~568 nm) solvents (Fig. 2(c)). The intensity of the absorbance peak in the unirradiated ethanol solution of **RHBIT** was slightly enhanced

Table 1 pH, absorption, and emission maxima and Stokes shift of **RHBIT** in different solvents before and after exposure to UV light with polarities and p$K_a$ values of respective screened common solvents. A blue color indicates variation in pH and wavelength values before and after exposure to short-wavelength UV light (254 nm)

| Solvent | Polarity | p$K_a$ | RHBIT before UV exposure | | | | RHBIT after UV exposure | | | |
|---|---|---|---|---|---|---|---|---|---|---|
| | | | pH | $\lambda_{Abs}$ (nm) | $\lambda_{Emi}$ (nm) | Stokes shift ($cm^{-1}$) | pH | $\lambda_{Abs}$ (nm) | $\lambda_{Emi}$ (nm) | Stokes shift ($cm^{-1}$) |
| Methanol | 0.762 | 15.5 | 7.8 | 382 | 427 | 2759 | 7.8 | 383 | 427 | 2690 |
| Ethanol | 0.654 | 15.9 | 4.4 | 560 | 589 | 880 | 4.4 | 560 | 589 | 880 |
| *n*-Propanol | 0.617 | 16.8 | 8.2 | 387 | 430 | 2584 | 8.2 | 384 | 430 | 2786 |
| *n*-Butanol | 0.586 | 16.1 | 7.7 | 386 | 432 | 2758 | 7.7 | 388 | 430 | 2625 |
| *N*,*N*-dimethylformamide | 0.386 | — | 11.2 | 393 | 433 | 2351 | 10.8 | 394 | 431 | 2179 |
| Dimethylsulfoxide | 0.444 | 35 | 12 | 396 | 435 | 2264 | 5.5 | 568 | 594 | 770 |
| Acetonitrile | 0.460 | 25 | 7.9 | 389 | 425 | 2177 | 7.8 | 388 | 425 | 2244 |
| 1,4-Dioxane | 0.164 | — | 7.4 | 385 | 430 | 2719 | 7.8 | 385 | 430 | 2719 |
| Ethylacetate | 0.228 | 25 | 6.7 | 384 | 426 | 2567 | 6.4 | 389 | 426 | 2232 |
| Tetrahydrofuran | 0.207 | — | 7.1 | 390 | 429 | 2331 | 7.1 | 394 | 430 | 2125 |
| Chloroform | 0.259 | 15.5 | 6.7 | 387 | 433 | 2745 | 3.3 | 557 | 432, 588 | 947 |
| Dichloromethane | 0.309 | — | 7.7 | 391 | 431 | 2374 | 3.5 | 558 | 433, 584 | 798 |

(0.04 units) after UV exposure and the absorbance changes after irradiation for $CHCl_3$, DCM, and DMSO correlated well with the color changes (colorless to pink under visible light and short-wavelength UV (254 nm)), which can be noted clearly in the photographs in Fig. 2(a2) and (a3). **RHBIT** in $CHCl_3$ and DCM manifested strong dual emission at 588 nm and 584 nm, and weak emission at 594 nm in DMSO along with the usual peak at 433 nm, while emission at ~589 nm for ethanol remains unchanged (Fig. 2(d)). $CHCl_3$ and DCM solutions of **RHBIT** show a highly emissive strong band at 584 nm due to the longer lifetime and higher quantum yield of the ring-open state. The variation in emission intensity at ~584–594 nm and the color changes after UV illumination in ethanol, DMSO, $CHCl_3$, and DCM solvents are clearly depicted in Fig. 3, and no considerable change in emission intensity after irradiation was observed in ethanol solvent. These spectral and color changes indicate that **RHBIT** isomerizes to a zwitterionic form by cleavage of the C–N bond in spironolactone resulting in an open form by a photo-induced ring-opening mechanism along with an extended conjugated structure with strong absorbance and emission intensities.[41] Moreover, the electron-withdrawing nitro group attached to the benzenoisothiazole moiety of **RHBIT** facilitates less conjugation into an extended conjugated structure; also chlorinated solvents like $CHCl_3$ and DCM have a hydrogen-bonding character; they are able to behave as H-bond donors.[42] Hence, **RHBIT** exhibits typical rhodamine spirolactam ring-opening behavior in the presence of acid and also under UV light illumination.[20] We have further studied the emission intensity of the newly formed photoinduced products at regular intervals for 48 h. After 48 h, the emission intensity decreased ~4-fold and 140-fold for $CHCl_3$ ($\lambda_{max,emi}$ = 588 nm) and DCM ($\lambda_{max,emi}$ = 584 nm) solutions, respectively (Fig. S8†). In contrast, the emission intensity remains unaltered for ethanol and DMSO and the color of the solutions remains light pink after subsequent storage in the dark, at room temperature for 5 days. In DMSO, the solvent pink color persists even after 2 months. This indicates that the photoresponsive behavior of **RHBIT** in $CHCl_3$ and DCM was reversible as they returned to their original states and irreversible in the case of DMSO and the color changes persevered for minutes to months, depending

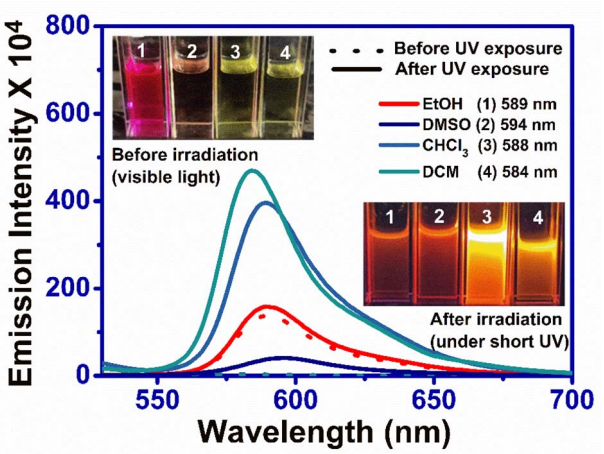


Fig. 3 Enhancement in emission intensity of **RHBIT** at ~584–594 nm in ethanol, DMSO, $CHCl_3$, and DCM after exposure to short-wavelength UV light (254 nm), showing intense orange emission in the case of chloroform and DCM. Inset shows a change in color variation before irradiation (photograph taken in visible light) and after exposure to UV (photograph taken in short-wavelength UV light).

upon the solvent medium. After irradiation, the $CHCl_3$ and DCM solutions of **RHBIT** were subjected to heating at 40–60 °C, and still the pink color of the solutions was retained, suggesting the thermal stability and irreversible photochromic feature of **RHBIT**. To gain mechanistic insight into the photochemical reaction of **RHBIT**, the $^1$H NMR spectra of **RHBIT** before and after UV exposure were recorded in $CDCl_3$. The $^1$H NMR spectrum showed a severe broadening of lines and the splitting pattern was unclear with UV light irradiation compared to that before irradiation (Fig. S9†). The color of the solution changed from yellow to prominent pink in deuterated $CDCl_3$ after short-wavelength UV illumination. From the spectral behavior, it is presumed that photoisomerization takes place from the closed ring to the open form[41] of **RHBIT** and a plausible mechanism for the photoinduced ring-opening process is proposed in Scheme 2. Variation of pH, quantum yield, and lifetime decay in the above-mentioned solvents, studied before and after UV irradiation, disclosed that pH in $CHCl_3$, DCM, and DMSO was reduced to an acidic range (3.3–5.5) (Table 1), which as mentioned before is evocative of strong protonation of the spirocyclic form of **RHBIT**, which further transforms to an open form in an acidic environment. Moreover, variation in pH was not observed for the remaining solvents before or after UV illumination.

The optical band gap of solid **RHBIT** was calculated using a Tauc plot before and after UV light irradiation and they were found to be similar, ~4.7 eV (before UV exposure) and 4.6 eV (after UV exposure) (Fig. S10(a) and (b)†), suggesting an insulating property of **RHBIT**. The absorption wavelength of solid **RHBIT** occurred at 433 nm along with a weak charge-transfer band at ~1681 nm, representing the weak charge-transfer interactions of ANB with the phenyl group of the xanthene moiety. Similar responses in the solid **RHBIT** suggested no photochemical reaction happening (Fig. S10(c)–(e)†). No prominent characteristic emission peak was observed.

The **RHBIT** molecule adopts two different isomers, with its ANB ring intact and with the ring-open form. The latter form is predominantly observed in an acidic medium. The highest occupied molecular orbital (HOMO) and the lowest unoccupied molecular orbital (LUMO) energies of both the forms of **RHBIT** are given in Fig. 4. The HOMO–LUMO energy gap decreases from 6.3 eV to 5.9 eV when the cyclized form changes to the open form. The strain in the cyclized form of **RHBIT** increases the energy of the individual frontier orbitals and also the HOMO–LUMO energy gap.

Natural transition orbital[43,44] (NTO) analysis was performed for thirty electronic excitations in the UV visible region from the ground state with the TDDFT method. In the cyclic form, the most intense band (corresponding to the TDDFT transition with the highest oscillator strength) is calculated for the excited state where the electronic transition is from HOMO−2 → LUMO+5 with a wavelength of 214 nm. The NTOs show that the electronic transitions are a combination of π–π* from the RHB moiety along with charge transfer from the RHB moiety to the $NO_2$ group of the ANB moiety, as shown in Fig. 5(a). This agrees well with the low-wavelength band in the absorbance data of the **RHBIT** system with most of the solvents. The $S_0 \rightarrow S_1$ excitation in the cyclic **RHBIT** is calculated at 401 nm, corresponding to the HOMO–LUMO transition, with zero oscillator strength (Fig. 5(b)). The corresponding NTO shows a charge transfer between π–π* of the RHB moiety to the ANB group of **RHBIT**. This forbidden transition at 401 nm confirms the absence of the high-wavelength band of the **RHBIT** system with most of the solvents. Unlike in the cyclic form, the most intense excitation

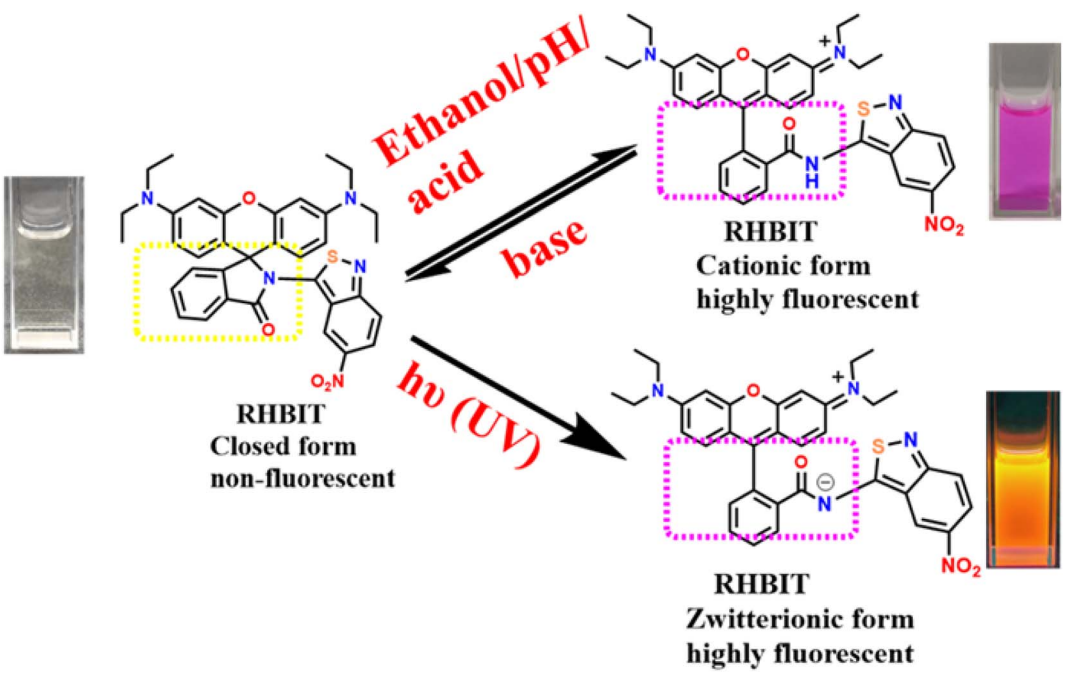


Scheme 2 Plausible mechanism of closed and open forms of RHBIT by external stimulation.

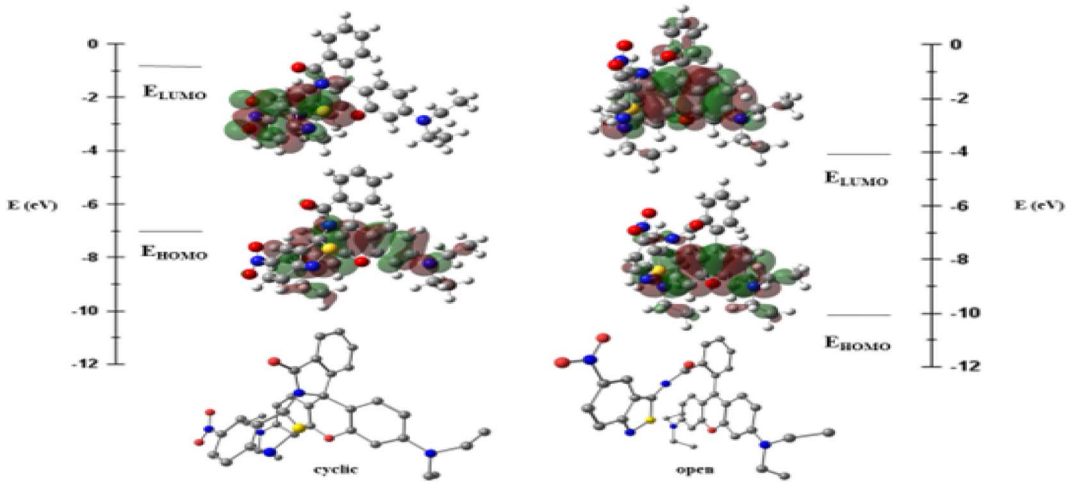


Fig. 4 The HOMO–LUMO energy diagram of the cyclized and open **RHBIT** system. The optimized structures, the calculated HOMO and LUMO energy levels, and the HOMO–LUMO energy gaps (in units of eV) are presented for cyclized and open forms.

in the open form of **RHBIT** is calculated for the $S_0 \rightarrow S_1$ transition with a wavelength of 424 nm. From the NTOs, we observe that the electronic transitions involve locally excited $\pi$–$\pi^*$ transition from the RHB moiety, as shown in Fig. 5(c). This high-wavelength low-energy band also agrees well with the absorbance data.

**3.3.3 Lifetime and quantum yield measurements.** Fluorescence intensity enhancement motivated us to examine fluorescence decay through excited-state lifetime studies. The resultant decay components before (Fig. S11(a)†) and after UV irradiation (Fig. S11(b) and (c)†) were analyzed as bi-exponential functions by adjusting the chi-squared value between 0.8 and 1.2. The decay parameters are listed in Table S8 (ESI†). The fluorescence lifetime decays of **RHBIT** in ethanol at ~589 nm before and after UV exposure were alike (1.16 ns and 1.11 ns) (Fig. S11(c)†), suggesting that the decay originated from a similar excited state. In contrast, the lifetime values for $CHCl_3$, DCM, and DMSO (~584–588 nm) solutions of **RHBIT** after UV irradiation had slightly higher values, *i.e.*, 2.4 ns, 3.4 ns, and 1.1 ns (Fig. S11(c)†), compared to the closed form *i.e.* before UV exposure (1.26 ns, 1.28 ns, 0.78 ns); these results suggest that the short-wavelength UV irradiation increases the lifetime values, which enhances the stability of the xanthylium cation representing the ring-opened state of **RHBIT**.[45] Hence, the accomplished results agreed with the steady-state fluorescence spectral data. The equations used for calculating average lifetime, radiative ($k_r$) and non-radiative ($k_{nr}$) decay constants, and quantum yield are provided in the ESI;† the values are tabulated in Table S8.† It is evident that the radiative decay constant and luminescence quantum yield of **RHBIT** in $CHCl_3$, DCM, and DMSO increase drastically after UV illumination; non-radiative decay values decrease but remain similar for the other solvents (Table S8†), in accordance with the variation trends of fluorescence intensities. Thus, an enormous enhancement in emission intensity is principally due to increased radiative decay values compared to radiationless relaxation.[46] The above results indicate the photoisomerization between fluorescence off and on states of **RHBIT** in the different solvents considered in the study.

**3.3.5 Protonation of RHBIT with *p*-toluene sulfonic acid.** To a greater extent, the switching between the closed ring and open form of **RHBIT** was demonstrated by sensing different

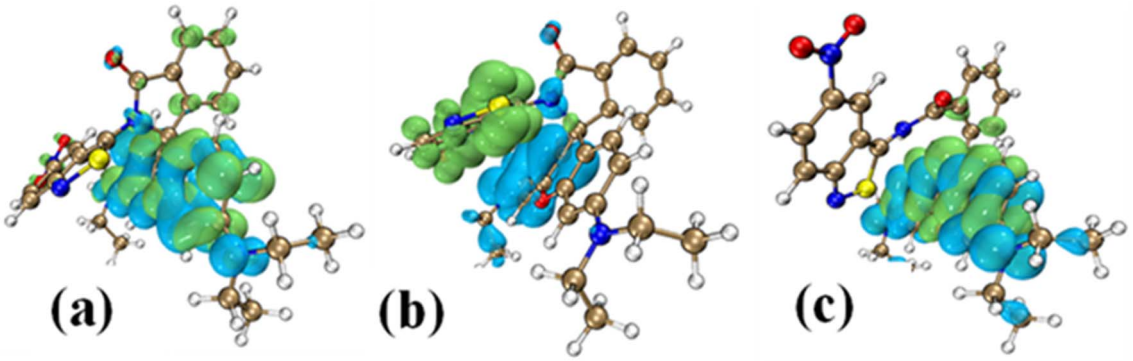


Fig. 5 The natural transition orbital (green: hole and cyan: electron) associated with the electronic excitation of cyclic **RHBIT** at (a) 214 nm and (b) 401 nm (with zero oscillator strength), and that of ring-open **RHBIT** at (c) 424 nm.

acids like HCl, $H_2SO_4$, $HNO_3$, benzoic acid, 4-chloro,3-nitrobenzoic acid, 4-aminobenzoic acid, anthranilic acid and *p*-toluene sulfonic acid (**PTSA**) through protonation of the nitrogen atom in the amide linkage. 40 μM of **RHBIT** in acetonitrile was treated with 50 μM of different acids, and the relevant absorbance, emission spectra were recorded (Fig. S12†). Characteristic absorption and emission peaks were not found in **RHBIT** above 500 nm; representing a non-fluorescent cyclized form. However, after the addition of the above-specified acids, strong absorption and emission peaks originated at 560 nm and ~585 nm, respectively, except for 4-aminobenzoic acid, and anthranilic acid with weak emission intensity. Among these, the emission intensity of **PTSA** with **RHBIT** at 585 nm was enhanced ~150-fold with respect to **RHBIT**. Furthermore, sensing studies were carried out with disparate concentrations of **PTSA** in acetonitrile without changing the concentration of the probe (40 μM). For each titration, 1800 μL of the probe and 200 μL of **PTSA** with concentrations of 10 to 120 μM were added to a 3 mL quartz cuvette. Absorption spectra revealed that $\lambda_{max}$ absorption is at 560 nm; (Fig. 6(a)); on excitation at 520 nm, an orange-red emissive peak at 585 nm was noticed for the open form of **RHBIT**, and simultaneously the intensity of the probe increased with an increase in the concentration of **PTSA** (Fig. 6(b)), designated to the extended π-conjugated planar structure of the open form. This results in complex formation by donating a proton from the sulfonic acid group of **PTSA** to the amide linkage of **RHBIT**, promoting the ring-opening mechanism. Recently, we realized that benzoisothiazole forms a simple protonated hydrogen-bonding complex with **PTSA**.[25] Also, herein, an enhanced emission intensity at 585 nm manifested a good linear relationship with the concentration of **PTSA** in the ~45 to 61 μM range, as shown in the inset of Fig. 6(b); the bright color change of the probe from colorless to prominent pink was pronounced in Fig. 6(c)–(e).

Moreover, the binding mechanism of **RHBIT** with **PTSA** is supported by FT-IR (Fig. S13(a)†) and $^1$H NMR spectra. A shift in the carbonyl (C=O) group stretching frequency was observed from 1716 $cm^{-1}$ (**RHBIT**) to 1591 $cm^{-1}$ (**RHBIT–PTSA**). The lower frequency shift resembles the stretching frequency of C=O in rhodamine B, indicating the open-ring form of rhodamine spirolactam through protonation by **PTSA**. To gain better insight into the ring-opening mechanism, we accomplished an $^1$H NMR titration experiment of **RHBIT** in $CDCl_3$ using a continuous titration method by adding different volumes (10–100 μL) of **PTSA** in DMSO-$d_6$. The peak shape of **RHBIT** becomes broadened and a slight downfield shift of the aliphatic and aromatic protons was observed. Both methyl and aromatic protons of **PTSA** were also recognized in the spectra after adding 100 μL of **PTSA**. A new signal at $\delta = \sim 11.4$ ppm was found, suggesting that the signal is due to the –*N*–H proton of the amide functionality, indicating the opening of **RHBIT** in the presence of **PTSA** (Fig. 7). The switching between closed and

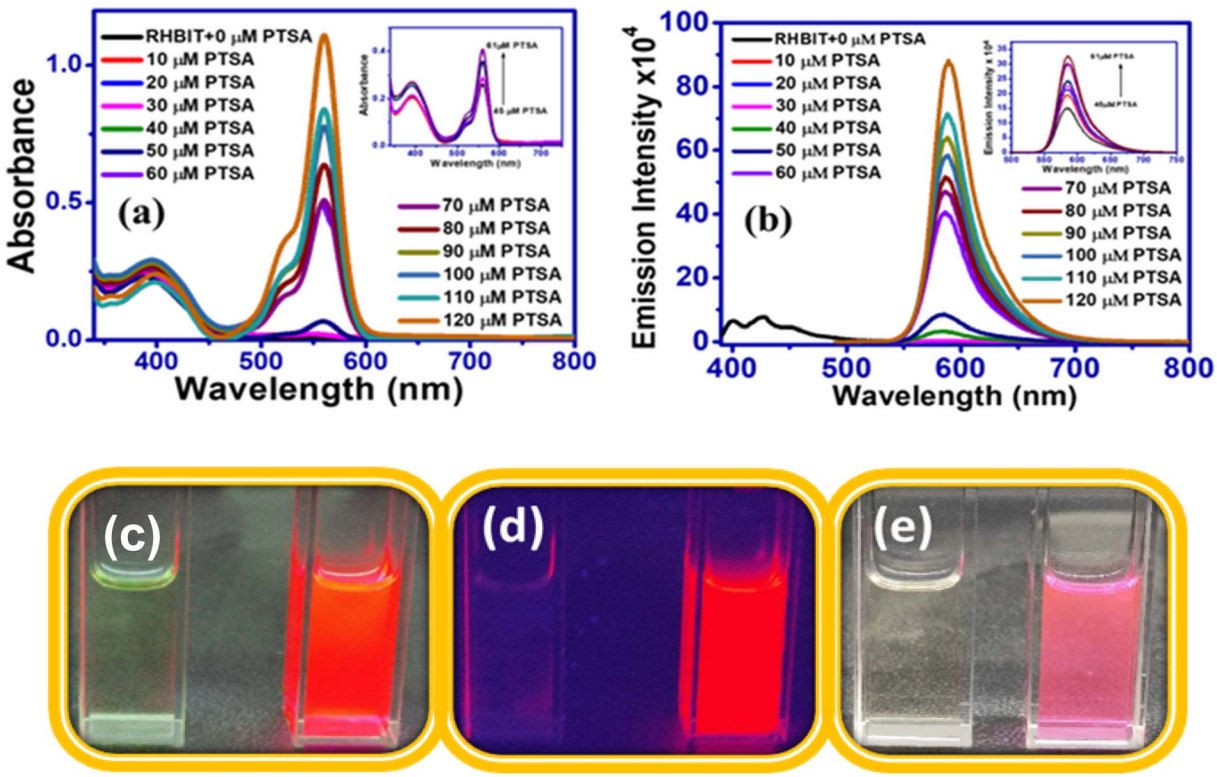


Fig. 6 The (a) absorption and (b) emission spectra of RHBIT (40 μM) on titration with different concentrations of PTSA (0–120 μM), depicting an increase in intensity with an increase in concentration. The inset figures represent an increase in intensities of absorbance and emission in the 45–61 μM range. (c), (d) and (e) display the colorimetric responses of pure RHBIT (left) and after adding PTSA (right) in short-wavelength UV, long-wavelength UV, and visible light, respectively.

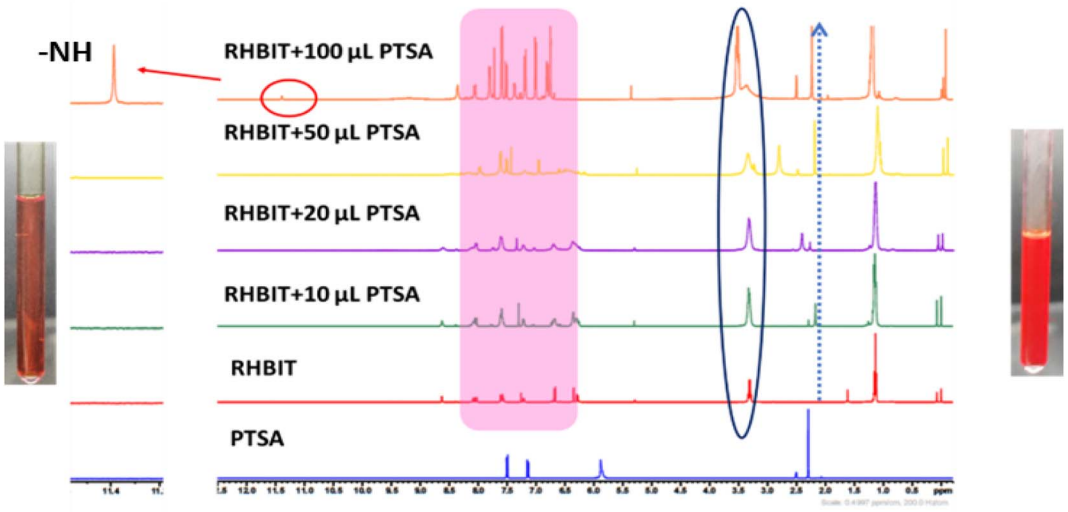


Fig. 7 The $^1$H NMR titration spectra of **RHBIT** with an increase in the concentration of **PTSA**. The variation in signals after the addition of **PTSA** is marked on the spectrum. Inset pictures show the color transformation (left) **RHBIT** after adding **PTSA**, (right) **RHBIT**–**PTSA**.

open forms of **RHBIT** with **PTSA** can be seen visually by a prominent color change to pink (Fig. 7), which clearly supports the involvement of the amide carbonyl oxygen in the ring-opening mechanism.[45] From the above observation, a plausible mechanism for the proton-induced ring-opening process in **RHBIT** is proposed in Scheme 2. Several attempts to crystallize **RHBIT**–**PTSA** were in vain. Acetonitrile solutions of **RHBIT** and **PTSA** at a ratio of 1 : 1 were mixed and heated gently at 50 °C and kept for evaporation at room temperature; after 3 days pale brown-colored crystals were formed at the bottom, while the supernatant solution was pink (Fig. S13(b)†), consistent with the spirocyclic form of **RHBIT**. A similar observation was reported by Fogerty *et al.* when they attempted to crystallize rhodamine B phenylene diamine dimer with HCl.[20]

*3.3.4.1 Limit of detection and binding stoichiometry of **RHBIT** with **PTSA**.* The sensitivity of **RHBIT** towards **PTSA** has been determined by estimating the limit of detection (LOD), as shown in Fig. 8(a). The limit of detection was calculated by the following method (LOD = $3\sigma/K$),[14] where $\sigma$ is the standard deviation for blank measurement ($\sigma = 72.81$) and $K$ is the slope of linear fitting lines of the titration data. To determine $\sigma$, the emission intensity values of the blank solutions were each measured thrice. The LOD value for **RHBIT** towards **PTSA** was calculated as 23 nM, suggesting that **RHBIT** is highly sensitive towards **PTSA** through the ring-opening mechanism *via* protonation. The binding stoichiometry between **RHBIT** and **PTSA** was evaluated by Job's method (Fig. 8(b)). A Job plot was constructed by considering the changes in absorption intensity ($Y$-axis) at 560 nm as a function of mole fraction ($X$-axis) of **PTSA** after adding it to **RHBIT** and the binding stoichiometry between **RHBIT** and **PTSA** was found to be 1 : 1.

Reversibility and regeneration of chemosensors play a key role in practical and bioimaging applications. Herein, to demonstrate the reversibility of **RHBIT** (25 ppm) in acetonitrile, **PTSA** (25 ppm) in acetonitrile and triethyl amine were introduced to the probe solution and the respective emission spectra were recorded. As mentioned above, **RHBIT** was non-fluorescent and colorless. When **PTSA** was added, the probe

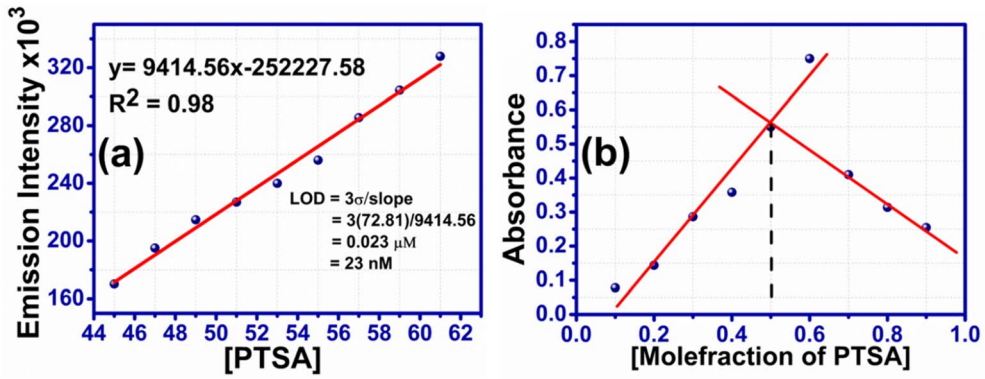


Fig. 8 (a) Limit of detection limit of **RHBIT** after the addition of **PTSA** considering the linear range from 45 to 61 µM. (b) Job's plot of **RHBIT** with **PTSA**, indicating 1 : 1 binding ratio.

formed strong complexation with **PTSA** through protonation, and fluoresced highly at ~592 nm, exhibiting a visually pink color. Later, triethylamine (TEA) (20 μL) was added to the solution containing the probe and **PTSA**. The experimental results showed that emission intensity was quenched at ~592 nm with the disappearance of the pink color due to the decomplexation of **RHBIT** by TEA, returning it to the ring-closed form (Fig. 9(a)). A similar experiment was executed after short-wavelength UV light irradiation of **RHBIT** in chloroform. Before UV exposure **RHBIT** shows an emission peak at ~433 nm representing a cyclized form; after irradiation at 254 nm UV light it shows an orange emission peak at ~585 nm, signifying the conversion of the cyclized form to the open-ring form. Upon further addition of small aliquots of TEA, the emission intensity was quenched at ~585 nm and there was a simultaneous increase in the emission peak at 433 nm, suggesting return of the open-ring form back to spirolactam. In the current situation, TEA push–pulls the open ring to the cyclized form (Fig. 9(b)). Therefore, **RHBIT** could be considered a potentially reversible chemosensor,[46] and, since switchable color changes could be visualized with the naked eye (Fig. 9), it could perhaps employed for information protection applications.

### 3.4 Thermal analysis and scanning electron microscopy images

The thermal stability of **RHBIT** was determined by thermogravimetric analysis (TGA) and DSC differential scanning calorimetry (DSC) (Fig. S14†). TGA analysis reveals that **RHBIT** was moisture free and thermally stable up to 294 °C; it then decomposed in a single step with a significant weight loss of 52.2%, corresponding to a mass of 323 g from the total mass of 619 g. A gradual weight loss eventuates when the temperature exceeds 294 °C (Fig. S14(a)†). This might be due to the thermal decomposition of two diethyl amino groups and the 3-nitro,-benzoisothiazole moiety in **RHBIT**.[47] Finally, the residual mass after the decomposition process was ~47.8% *i.e.*, 296 g corresponding to the xanthene moiety with the carbonyl phenyl group. DSC analysis (Fig. S14(b)†) illustrates a sharp melting peak at ~293 °C, indicating the purity and thermal stability of **RHBIT**. The decomposition temperature from TGA and melting point from DSC were in good agreement. To gain insight into the morphology, 25 ppm of **RHBIT** in acetonitrile, isopropanol, *n*-butanol and DMF solutions were each separately drop-cast on silicon wafers and dried at room temperature for 48 hours. The morphology in acetonitrile solution depicted flowers at 5 μm magnification, while bent petal-like structures were observed at 20 and 100 μm (Fig. S15†). Aggregates were noted in i-propanol, *n*-butanol and DMF solutions at 1 μm. Incompatible morphologies could probably be due to different rates of solvent evaporation. Consequently, the molecular interactions with solvent/diffusion capability result in molecular assemblies and emerge in different growth kinetics.[47]

### 3.5 Application of RHBIT as a rewritable platform

The fluorescence switching properties with magnificent bright color changes inspire the use of these materials as a platform for reusable optical reading and to detect base analytes. To further confirm the photoresponsive property and reversibility of **RHBIT**, we distributed a chloroform/DCM solution of **RHBIT** on a small piece of paraffin film placed on a glass slide and wrote "BITS" (the short form of the name of our institute) with a small capillary on the film, as shown in Fig. 10(a). Then the film was exposed to short-wavelength UV light for 5 min by placing it in a UV chamber. A swift intense color change was observed from "colorless to prominent pink" in the word "BITS". This represents a ring-open form of **RHBIT** after irradiation by 254 nm short-wavelength UV light. The pink letters were erased by overwriting them with TEA. A similar phenomenon was observed on a flower-shaped cut paraffin film. The flower was placed on a Petri dish, and **RHBIT** chloroform solution dropped on it. The flower film emits a visually intense pink color under short-wavelength UV light (254 nm). The film was preserved on a Petri dish and dripped with TEA; consequently, "pink changes to colorless" (Fig. 10(b)). This scrutiny reveals the visible transformations of closed–open–closed isomerization of spirocyclic **RHBIT**. Thus, a striking and rewritable bright color change is easily seen in very affordable small molecules. Likewise, different patterns can be printed

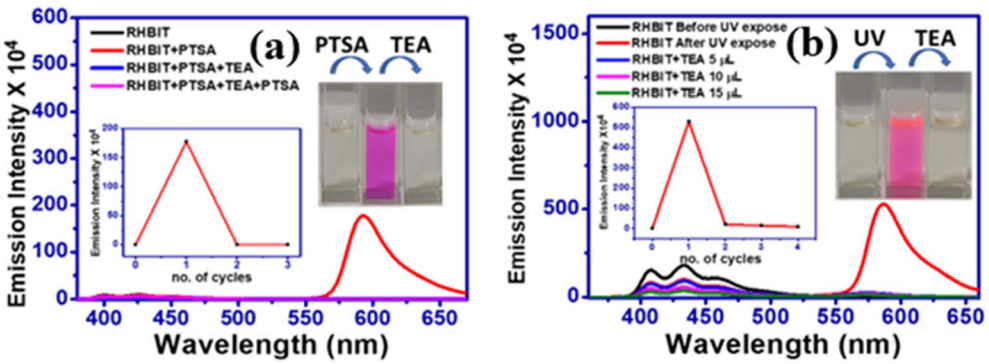


Fig. 9 Changes in the emission intensity of RHBIT (40 μM) in ACN (1500 μL): (a) upon alternate addition of a fixed amount of PTSA (500 μL) and TEA (20 μL); (b) upon the addition of different volumes of TEA (5, 10, 15 μL) to RHBIT (2000 μL) after UV irradiation. Insets in (a), (b) show the reversibility along with the fluorescence response *vs.* no. of cycles, performed at an emission wavelength 585 nm and the colorimetric response of RHBIT.

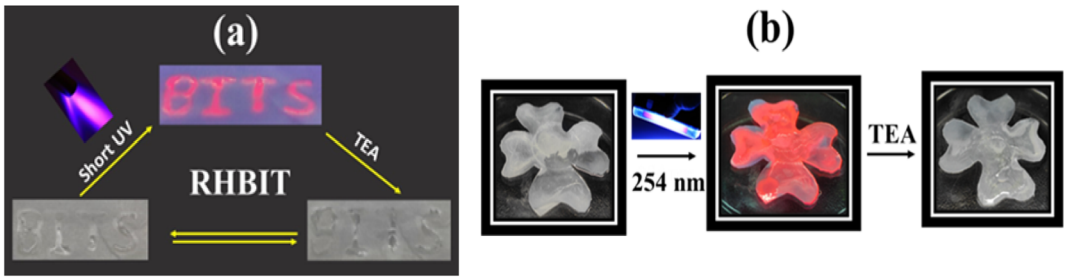


Fig. 10 Demonstration of writing and erasing on paraffin film: (a) writing and erasing process carried out on a film with chloroform solution of RHBIT and TEA under 254 nm UV light. (b) Images of flower-shaped film and its color appearance of RHBIT after 254 nm short-wavelength UV exposure followed by dropping of TEA.

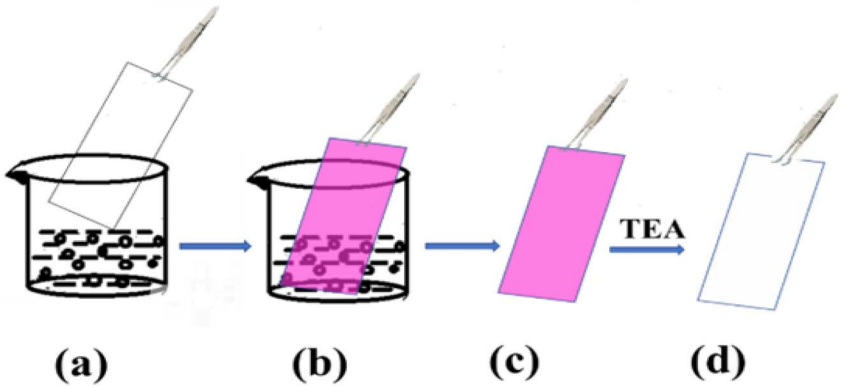


Fig. 11 Schematic representation of silica-coated TLC plates (a) dipped in chloroform solution of RHBIT. (b) and (c) The TLC plate turned a pink color after dipping in chloroform solution. (d) The TLC plate change to colorless when dipped in/exposed to TEA.

and easily erased on paraffin films, indicating that **RHBIT** can serve as a security ink for photopatterning, smart labels, indicators, packing materials for laboratory purposes, and medical diagnostics.

The switching between on/off states of **RHBIT** by acid/base treatment is also achieved by TLC-coated strips. A silica-coated TLC plate was dipped in **RHBIT** chloroform solution and taken out, and the color of the plate turned pink (Fig. 11). The acidic nature of the TLC silica strips induces protonation of the spirolactam nitrogen group, further leading to simultaneous ring-opening and a transition from the colorless cyclized form to the pink-colored open-state form.[48] Furthermore, the pink-colored TLC plate, when dipped in or exposed to TEA turns colorless. TEA deprotonated the ring-open form and returned it to the colorless spirocyclic form. Therefore, **RHBIT** could be successfully applied as a fluorescent turn-on sensor on paraffin film and TLC plates.

## 4 Conclusion

In summary, we report the successful synthesis and detailed characterization of a novel multi-functional (multi-stimuli-responsive) molecular material **RHBIT** *via* fusing low-cost RHB with ANB. **RHBIT** showcased selective ethanol/pH responsiveness, acidochromism, and UV light stimulation; evidenced by off–on switching and emission color changes by the naked eye/under UV light. A single-crystal X-ray diffraction study of **RHBIT** reveals a spirolactam ring structure. Short-wavelength UV light (254 nm) stimulates the **RHBIT** into a ring-open form, mostly in chlorinated solvents like $CHCl_3$, DCM, and DMSO (the color persists even after 2 months) with long lifetimes. The DFT and TDDFT calculations support the absorption properties of the closed and open forms. The acid chromic behavior of **RHBIT** and its reversible switching on–off nature with acid/base could be exploited for information protection applications. **RHBIT** exhibited high sensitivity toward *p*-toluene sulfonic acid with a limit of detection of 23 nM and shows 1 : 1 binding stoichiometry between **RHBIT** and **PTSA**. The outcome of this work reveals that the fusion of RHB with a fused heterocycle ring accompanied by an electron-withdrawing substituent and the primary amino group could provide a new strategy to accomplish a broad approach for the development of multi-stimuli-responsive molecular fluorescent switches.

## Author contributions

Himabindu Battula: Investigation, Methodology, Data curation, Writing-rough draft. Moromi Nath: DFT, TD-DFT calculations, Formal analysis, Documentation. Sabyashachi Mishra: DFT, TD-DFT calculations, Write up, Editing of computational study. Subbalakshmi Jayanty: Supervision, Writing-original draft,

review and editing, Investigation, Methodology, Formal analysis, Crystallography, validation, Funding acquisition, Project administration, and organization.

## Conflicts of interest

The authors declare no conflict of interest.

## Acknowledgements

SJ thanks SERB-DST (Reference No. DST-EMR/2016/002209) Govt. India for the financial support. The authors gratefully acknowledge the Central Analytical Laboratory (CAL) facility provided by the BITS-Pilani, Hyderabad campus. The DST-FIST grant facility is also highly accredited. M. N. acknowledges IIT Kharagpur for fellowship. S. M. acknowledges SERB, DST, Government of India (SR/FST/CSII-026/2013). This work employed the resources of the Paramshakti supercomputing facility of IIT Kharagpur established under the National Supercomputing Mission of the Government of India and supported by CDAC, Pune.

## References

1 W. Du, X. Liu, L. Liu, J. W. Y. Lam and B. Z. Tang, *ACS Appl. Polym. Mater.*, 2021, **3**, 2290–2309.
2 Y. Li, Q. Peng, S. Li, C. Yang, J. He, Q. Hu and K. Li, *Dyes Pigm.*, 2019, **171**, 107750–107756.
3 L. Wang and Q. Li, *Chem. Soc. Rev.*, 2018, **47**, 1044–1097.
4 M. K. Lee, P. Rai, J. Williams, R. Twieg and W. E. Moerner, *J. Am. Chem. Soc.*, 2014, **136**, 14003–14006.
5 S. K. Patel, J. Cao and A. R. Lippert, *Nat. Commun.*, 2017, **8**, 15239–15247.
6 M. Ansari, R. Bera, S. Mondal and N. Das, *ACS Omega*, 2019, **4**, 9383–9392.
7 P. Agostinis, K. Berg, K. A. Cengel, T. H. Foster, A. W. Girotti, S. O. Gollnick, S. M. Hahn, M. R. Hamblin, A. Juzeniene, D. Kessel, M. Korbelik, J. Moan, P. Mroz, D. Nowis, J. Piette, B. C. Wilson and J. Golab, *Ca-Cancer J. Clin.*, 2011, **61**, 250–281.
8 Y. Zhu, C. Gu, Y. Miao, B. Yu, Y. Shen and H. Cong, *J. Mater. Chem. B*, 2019, **7**, 6576–6584.
9 A. Li, N. Chu, L. Huang, L. Han, Y. Geng, S. Xu, L. Pan, H. Cui, W. Xu and Z. Ma, *Dyes Pigm.*, 2019, **162**, 831–836.
10 K. Zheng, Q. Zou, Y. Yang, Y. Mao, J. Zhang and J. Cheng, *Ind. Eng. Chem. Res.*, 2018, **57**, 13283–13290.
11 M. Natali and S. Giordani, *Chem. Soc. Rev.*, 2012, **41**, 4010–4029.
12 G. Berkovic, V. Krongauz and V. Weiss, *Chem. Rev.*, 2000, **100**, 1741–1754.
13 V. W. W. Yam, J. K. W. Lee, C. C. Ko and N. Zhu, *J. Am. Chem. Soc.*, 2009, **131**, 912–913.
14 H. Battula, S. Muduli, S. Priyanka Bandi, S. Kapoor, S. Mishra, H. Aggarwal, V. Vamsi Krishna Venuganti and S. Jayanty, *J. Photochem. Photobiol. Chem.*, 2022, **426**, 113748–113766.
15 H. Battula, S. Bommi, Y. Bobde, T. Patel, B. Ghosh and S. Jayanty, *J. Photochem. Photobiol.*, 2021, **6**, 100026–100038.
16 M. Mathivanan, B. Tharmalingam, O. Anitha, C. H. Lin, V. Thiagarajan and B. Murugesapandian, *Mater. Chem. Front.*, 2021, **5**, 8183–8196.
17 Y. Li, Z. Feng, Y. Li, W. Jin, Q. Peng, P. Zhang, J. He and K. Li, *Spectrochim. Acta Mol. Biomol. Spectrosc.*, 2020, **230**, 118069–118076.
18 K. H. Knauer and R. Gleiter, *Angew. Chem., Int. Ed.*, 1977, **16**, 113.
19 J. Fölling, V. Belov, R. Kunetsky, R. Medda, A. Schoenle, A. Egner, C. Eggeling, M. Bossi and S. W. Hell, *Angew. Chem., Int. Ed.*, 2007, **46**, 6266–6270.
20 B.-F. C. Stratton, A. J. Pierre, E. A. Riser, N. J. Grinalds, C. W. Edwards, A. M. Wohlwend, J. S. Bauer, R. J. Spera, L. S. Pferdmenges, K. M. Griffith, B. W. Hunter, P. Bobadova-Parvanova, C. S. Day, P. M. Lundin and K. H. Fogarty, *J. Phys. Chem. A*, 2022, **126**, 4211–4220.
21 B. Li, U. Haris, M. Aljowni, A. Nakatsuka, S. K. Patel and A. R. Lippert, *Isr. J. Chem.*, 2021, **61**, 244–252.
22 W. L. Czaplyski, G. E. Purnell, C. A. Roberts, R. M. Allred and E. J. Harbron, *Org. Biomol. Chem.*, 2014, **12**, 526–533.
23 L. Huang, Y. Qiu, C. Wu, Z. Ma, Z. Shen and X. Jia, *J. Mater. Chem. C*, 2018, **6**, 10250–10255.
24 (*a*) T. Kaleemullah, M. Ahmed and H. K. Sharma, *J. Chem. Pharm. Res.*, 2012, **4**, 483–490; (*b*) G. E. Taylor, M. Gosling and A. Pearce, *J. Chromatogr., A*, 2006, **1119**, 231–237.
25 H. Battula, S. A. Nahata, L. D. Patnaik, S. Ranga and S. Jayanty, *J. Mol. Struct.*, 2021, **1225**, 129090–129100.
26 L. J. Bourhis, O. v. Dolomanov, R. J. Gildea, J. A. K. Howard and H. Puschmann, *Acta Crystallogr. A*, 2015, **71**, 59–75.
27 G. M. Sheldrick, *SHELXTL. Version 6.10*, Bruker AXS Inc., Madison, Wisconsin, USA, 2000.
28 G. M. Sheldrick, *SHELXS97 and SHELXL97*, University of Göttingen, Germany, 1997.
29 R. Dennington, T. A. Keith, and J. M. Millam, *Gaussview Version 6*, Semichem Inc., Shawnee Mission KS, 2019.
30 R. G. Parr, Density functional theory of atoms and molecules, in *Horizons of quantum chemistry*, Springer, 1980, pp. 5–15.
31 M. J. Frisch, G. W. Trucks, H. B. Schlegel, G. E. Scuseria, M. A. Robb, J. R. Cheeseman, G. Scalmani, V. Barone, G. A. Petersson, H. Nakatsuji, X. Li, M. Caricato, A. V. Marenich, J. Bloino, B. G. Janesko, R. Gomperts, B. Mennucci, H. P. Hratchian, J. V. Ortiz, A. F. Izmaylov, J. L. Sonnenberg, D. Williams-Young, F. Ding, F. Lipparini, F. Egidi, J. Goings, B. Peng, A. Petrone, T. Henderson, D. Ranasinghe, V. G. Zakrzewski, J. Gao, N. Rega, G. Zheng, W. Liang, M. Hada, M. Ehara, K. Toyota, R. Fukuda, J. Hasegawa, M. Ishida, T. Nakajima, Y. Honda, O. Kitao, H. Nakai, T. Vreven, K. Throssell, J. A. Montgomery Jr, J. E. Peralta, F. Ogliaro, M. J. Bearpark, J. J. Heyd, E. N. Brothers, K. N. Kudin, V. N. Staroverov, T. A. Keith, R. Kobayashi, J. Normand, K. Raghavachari, A. P. Rendell, J. C. Burant, S. S. Iyengar, J. Tomasi, M. Cossi, J. M. Millam, M. Klene, C. Adamo, R. Cammi, J. W. Ochterski, R. L. Martin, K. Morokuma,

O. Farkas, J. B. Foresman and D. J. Fox, *Gaussian 16 Revision C.01*, Gaussian Inc., Wallingford CT, 2016.
32 J. da Chai and M. Head-Gordon, *Phys. Chem. Chem. Phys.*, 2008, **10**, 6615–6620.
33 M. J. Frisch, J. A. Pople and J. S. Binkley, *J. Chem. Phys.*, 1984, **80**, 3265–3269.
34 T. Lu and F. Chen, *J. Comput. Chem.*, 2012, **33**, 580–592.
35 A. Pipattanawarothai and T. Trakulsujaritchok, *Dyes Pigm.*, 2020, **173**, 107946–107955.
36 F. Ali, S. Saha, A. Maity, N. Taye, M. K. Si, E. Suresh, B. Ganguly, S. Chattopadhyay and A. Das, *J. Phys. Chem. B*, 2015, **119**, 13018–13026.
37 M. Tian, X. Peng, J. Fan, J. Wang and S. Sun, *Dyes Pigm.*, 2012, **95**, 112–115.
38 B. Bag and A. Pal, *Org. Biomol. Chem.*, 2011, **9**, 915–925.
39 H. Li, H. Guan, X. Duan, J. Hu, G. Wang and Q. Wang, *Org. Biomol. Chem.*, 2013, **11**, 1805–1809.
40 R. C. Weast, *Handbook of Data on Organic Compounds, Vol. I and II*, CRC Press, Boca Raton/Florida, 1985.
41 M. Tanioka, S. Kamino, N. Koga and D. Sawada, *J. Mater. Chem. C*, 2020, **8**, 543–549.
42 A. Jordan, P. Stoy and H. F. Sneddon, *Chem. Rev.*, 2021, **121**, 1582–1622.
43 R. L. Martin, *J. Chem. Phys.*, 2003, **118**, 4775–4777.
44 R. Zhou and Y. Kanai, *J. Chem. Phys.*, 2021, **154**, 054107–054115.
45 A. Dhara, N. Guchhait and S. K. Kar, *J. Fluoresc.*, 2015, **25**, 1921–1929.
46 H. Lin, X. Chang, D. Yan, W. H. Fang and G. Cui, *Chem. Sci.*, 2017, **8**, 2086–2090.
47 A. Syed, S. Mishra and S. Jayanty, *J. Fluoresc.*, 2022, **32**, 115–124.
48 H. F. Nour and T. el Malah, *New J. Chem.*, 2020, **44**, 6068–6074.